



Exotic nuclei/Les noyaux exotiques

# The origin of the Ca–Ti–Cr–Fe–Ni isotopic anomalies in the inclusion EK-1-4-1 of the Allende meteorite

Olivier Sorlin<sup>a</sup>, L. Gaudefroy<sup>a</sup>, Karl-Ludwig Kratz<sup>b</sup>, Thomas Rauscher<sup>c</sup><sup>a</sup> Institut de physique nucléaire, IN2P3-CNRS, 91406 Orsay cedex, France<sup>b</sup> Institut für Kernchemie, Universität Mainz, Fritz-Strassmann-Weg 2, 55128 Mainz, Germany<sup>c</sup> Departement für Physik und Astronomie, Universität Basel, Klingelbergstrasse 82, CH-4056 Basel, Switzerland

Presented by Guy Laval

## Abstract

The origin of the correlated Ca–Ti–Cr–Fe–Ni isotopic anomalies in the Ca–Al-rich inclusion of the EK-1-4-1 of the Allende is a longstanding puzzle. The search for a stellar environment which could explain the enrichment of neutron-rich stable Ca–...–Ni isotopes in a self-consistent way requires nuclear physics data far from stability. Recent experimental data have been obtained in the region of the shell closures  $N = 28$  and  $N = 40$ , where the possible progenitors of these nuclei are found. Astrophysical network calculations have been updated by including the new  $\beta$ -decay properties and microscopic predictions of neutron-capture cross sections. Interplay between nuclear structure far from stability and the observed isotopic anomalies is especially evident for the high entropy ( $S \simeq 150$ ) scenario which would characterize the neutrino-driven wind in a type II supernova. **To cite this article:** O. Sorlin *et al.*, *C. R. Physique 4* (2003).

© 2003 Académie des sciences. Published by Éditions scientifiques et médicales Elsevier SAS. All rights reserved.

## Résumé

**Compréhension des anomalies isotopiques en Ca–Ti–Cr–Fe–Ni dans l’inclusion EK-1-4-1 de la météorite d’Allende.** L’origine des anomalies isotopiques corrélées en Ca–Ti–Cr–Fe–Ni dans l’inclusion EK-1-4-1 de la météorite d’Allende reste un mystère depuis une vingtaine d’années. La recherche d’un environnement stellaire qui peut expliquer de tels enrichissements en isotopes riches en neutrons de Ca–...–Ni requiert la connaissance de données de structure nucléaire loin de la vallée de stabilité. Des résultats récents ont été obtenus autour des fermetures de couches nucléaires  $N = 28$  et  $N = 40$ , où les générateurs potentiels de ces noyaux se trouvent probablement. Des calculs astrophysique en réseau ont été remis à jour en utilisant les nouvelles données de décroissance  $\beta$  et les calculs de capture de neutrons. La correspondance entre la structure des noyaux loin de la stabilité et les abondances observées est remarquable, en particulier dans le cas où ces anomalies isotopiques seraient produites lors d’une explosion de supernova de type II. **Pour citer cet article :** O. Sorlin *et al.*, *C. R. Physique 4* (2003).

© 2003 Académie des sciences. Published by Éditions scientifiques et médicales Elsevier SAS. All rights reserved.

**Keywords:**  $\beta$ -decay; Nuclear structure; Isotopic anomalies; Supernovae

**Mots-clés :** Décroissance  $\beta$ ; Structure nucléaire; Anomalies isotopiques; Supernovae

## 1. Introduction

The quest for the origin of the chemical elements has been a fascinating subject of philosophical, theological and scientific debates for centuries. The first decisive attempt to interpret the observed elemental composition from nuclear physics concepts

*E-mail addresses:* [sorlin@ipno.in2p3.fr](mailto:sorlin@ipno.in2p3.fr) (O. Sorlin), [klkratz@vkcmzd.chemie.uni-mainz.de](mailto:klkratz@vkcmzd.chemie.uni-mainz.de) (K.-L. Kratz), [Thomas.Rauscher@unibas.ch](mailto:Thomas.Rauscher@unibas.ch) (T. Rauscher).

was made by the fundamental paper of Burbidge, Burbidge, Fowler and Hoyle [1]. This work sets the starting point of Nuclear Astrophysics, an interdisciplinary field where astronomical observations, astrophysical modelling, meteoritic research, and nuclear physics merge. The credibility of any nucleosynthesis model must be checked against observations. The Sun was for a long time considered as a suited choice for this purpose, being the only sample for which we can determine a well defined isotopic composition throughout the periodic table of the elements. This point is crucial since the final isotopic abundances reflect the nuclear reactions in which they were formed. However, several stellar processes mixed during the formation of the protosolar nebula and built up the solar elemental abundance. It is, therefore, almost impossible to disentangle the various nucleosynthesis events which occurred in the solar system prior to its formation.

There is an active search for weakly mixed abundances which contain contributions from only a few sites. One possibility is to observe stars formed at the beginning of the galactic evolution, when very little nucleosynthetic processes had yet occurred. During galactic chemical evolution, the content of elements heavier than H and He in the interstellar medium is increased by stellar hydrostatic and explosive burning processes. Thus, the abundance ratios such as O/H or Fe/H can be used as indicators for the amount of nucleosynthetic processing which occurred for the material found in a given star. The discovery of ultra metal-poor (UMP) stars in the galactic halo ( $\text{Fe}/\text{H} \leq 1/1000$  of the Sun) has been a major breakthrough in astronomy, revealing the galactic composition at an early age [2–5].

Another possibility is brought by the abundance patterns of certain refractory inclusions of meteorites which exhibit large isotopic anomalies with respect to solar data. These observations indicate that their abundances have not been completely dissolved when incorporated into the solar nebula. They still carry fingerprints of the precursor exploding star from which pieces of matter have been ejected. They subsequently cooled and condensed into microscopic grains traveling through the interstellar medium, being eventually enclosed in other material, forming solid rocks and collected on Earth in the form of meteorites.

About two decades ago, G.J. Wasserburg and his group at Caltech identified correlated isotopic anomalies for the neutron-rich  $^{48}\text{Ca}$ ,  $^{50}\text{Ti}$  and  $^{54}\text{Cr}$  isotopes in peculiar refractory inclusions of the Allende meteorite [6,7]. As an example, the  $^{48}\text{Ca}/^{46}\text{Ca}$  ratio was found to be 250, a factor of 5 larger than in the solar system. About ten years after, other anomalies were discovered in  $^{58}\text{Fe}$  and  $^{64}\text{Ni}$  [8,9] in the same inclusions. It was concluded that these highly unusual isotopic compositions indicated late-stage nucleosynthesis processes which preceded the formation of the solar nebula. However, astrophysical models existing at that time encountered severe difficulties when trying to reproduce these observed anomalies, in particular those in the EK-1-4-1 inclusions. As already suggested in 1977, the key for describing these non-standard abundances reside in an improved knowledge of the relevant nuclear-physics parameters around the doubly magic  $^{48}\text{Ca}$ .

The present paper first depicts the most plausible astrophysical scenarii to account for these correlated isotopic anomalies in a self-consistent way. These scenarii require the knowledge of key nuclear structure parameters for nuclei far off stability, as  $\beta$ -decay half-lives, masses and neutron-capture cross sections. Experimental efforts on the progenitors of  $^{48}\text{Ca}$  and  $^{64}\text{Ni}$  are presented in the next sections. Special emphasis will be put on  $\beta$ -decay studies. The possibility to determine neutron-capture cross sections on unstable nuclei, and hereafter simulate neutron captures in exploding stars, is an important issue offered by radioactive nuclear beams. This perspective will be discussed in Sections 3 and 4.

## 2. Astrophysical scenarii

### 2.1. Neutron-capture processes in stars

The relative abundances of nuclides beyond Fe show a distinct pattern carrying imprints of the processes creating them. One can see a smooth fall-off beyond Fe on which three distinct twin peaks are superimposed, each with a narrow width at stable nuclides with magic neutron numbers  $N = 50, 82,$  and  $126,$  and a broader peak shifted to slightly lower mass numbers (Fig. 1). This indicates the existence of (at least) two components, attributed to slow (s) and rapid (r) neutron-capture nucleosynthesis.

The s process operates in red giants at relatively low neutron density of about  $10^8 \text{ cm}^{-3}$ , with neutron capture lifetimes on seed nuclei typically longer than  $\beta$ -decay lifetimes  $T_{1/2}$ . As a consequence, the s-process path follows the valley of stability and isotopes with small neutron-capture ( $n, \gamma$ ) cross section  $\sigma_n$  are greatly enhanced [10]. Small ( $n, \gamma$ ) cross sections are encountered for closed shell nuclei, where the s-process peaks – right part of a twin peak – are built at atomic masses  $A = 88, 140,$  and  $208.$  This neutron-capture process could have produced the neutron-rich  $^{46}\text{Ca}$  and  $^{48}\text{Ca}$  from a  $^{40}\text{Ca}$  seed, but it has to bridge the radioactive nuclei  $^{45}\text{Ca}$  ( $T_{1/2} = 162$  days) and  $^{47}\text{Ca}$  (4.5 days). Even if this condition could be fulfilled when assuming a relatively large stellar neutron density, a large/low  $\sigma_n$  should be found at masses  $A = 46, 47/A = 48$  in order to obtain a large overabundance of  $^{48}\text{Ca}$ . Measurements of  $\sigma_n$  have been performed for  $^{46}\text{Ca}$  and  $^{48}\text{Ca}$  [11], and it was concluded that even the ‘normal’ solar abundance ratio  $^{48}\text{Ca}/^{46}\text{Ca} = 53$  could not be reproduced. Even if  $^{48}\text{Ca}$  could be produced, it is easily destroyed by neutron-captures due to its large  $\sigma_n$ -value. This striking feature is rather unexpected for a closed shell

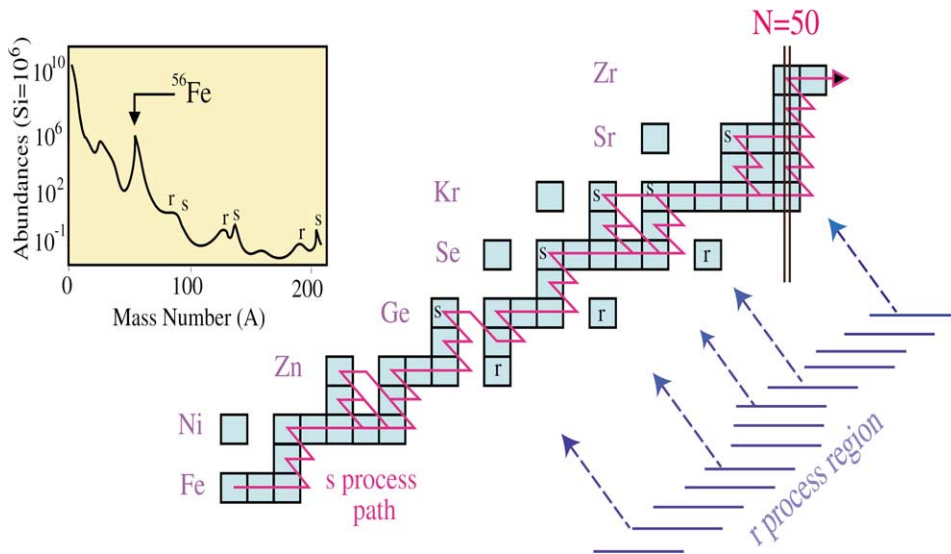


Fig. 1. Schematic view of the neutron-capture processes which account for the elements above iron. The observed abundance curve of the elements is shown in the inset. Three twins peaks witness the existence of *s* (slow) and *r* (rapid) neutron-capture nucleosynthesis. (Adapted from [10].)

nucleus. It is explained by the intrinsic nuclear structure of  $^{49}\text{Ca}$  which favor this neutron-capture rate (see Section 3.2 for details).

The *r* process occurs at high neutron densities  $10^{19-24} \text{ cm}^{-3}$ , presumably during the explosion of supernovae. The *r* path develops far off stability where the neutron-separation energies are as small as 2–3 MeV. At these locations, photodisintegrations ( $\gamma, n$ ) hamper further neutron-captures and the *r* process waits for the  $\beta$ -decay to the higher element. Nuclei are also accumulated at major neutron shell-closures (same  $N$ , but lower  $Z$  as compared to the *s* process), before the neutron-separation energy  $S_n$  drops by some MeV [12,13]. The corresponding abundance peaks are present at lower masses  $A$  compared to the related *s*-process maxima.

The hitherto discovered UMP stars [2–5] exhibit an almost pure *r*-like abundance pattern given the fact that *s*-process requires Fe seed nuclei on which neutron-capture could proceed. More strikingly, a solar-like *r*-abundance pattern has been observed in all UMP stars for heavy-mass nuclei ( $A > 130$ ), although they stem from very different regions of the galactic halo. These observations could suggest that very similar stellar conditions in terms of density, temperature, and mass range have occurred through years to produce these *r*-elements. It could also indicate that nuclear structure has a strong impact to confine the *r*-progenitors into a limited range of mass even for a possibly large variety of stellar conditions. Below  $A = 130$ , this remarkable agreement between the scaled solar abundances and the UMP stars is no longer valid and a large scatter in the  $A < 130$  abundance pattern is observed between the UMP stars. The missing part of the solar pattern reflects the need for a second ‘weak’ *r*-process. Thus, the light and heavy elements could be produced on different Galactic timescales and come from supernovae of different mass ranges. Based upon meteoritic data, Wasserburg et al. [14] have also suggested that two *r*-processes should exist, with a mass separation near  $A = 140$ , i.e., near Ba. This weak *r*-process could extend down to light masses, and be responsible for the observation of correlated isotopic anomalies in the neutron-rich  $^{48}\text{Ca}$ – $^{50}\text{Ti}$ – $^{54}\text{Cr}$ – $^{58}\text{Fe}$ – $^{64}\text{Ni}$  nuclei in certain inclusions of meteorites. The observation of light elements in UMP has been hitherto limited to Ge elements (Fig. 2), but it is foreseen to reach lighter elements in a near future.

## 2.2. Astrophysical network calculations

Calculations have been made with a time-dependent parametrized study to simulate appropriate explosive supernovae conditions. There, a hot blob of matter composed of neutrons, protons and  $\alpha$ -particles initially at a temperature  $T = 10^{10} \text{ K}$  expands adiabatically with a velocity of  $4500 \text{ km s}^{-1}$  and cools. This medium is characterized by an entropy  $S (\propto 4/3T^3/\rho)$ , a baryonic density  $\rho$  and a proton to nucleon ratio  $Y_e$  [15]. As the explosion develops, nucleons and  $\alpha$ -particles progressively combine to form heavier nuclei, typically up to iron. The Ca–Ti–Cr–Fe–Ni nuclei could be produced during this phase. The mean velocity of charged particles is shaped with a Maxwell–Boltzmann distribution whose mean energy scales with the stellar temperature. As the temperature decreases, reactions with  $\alpha$ -particles start to be inhibited because their energy is not sufficient to overcome the Coulomb barrier of the newly produced nuclei. This freeze-out of charged particles occurs especially at high

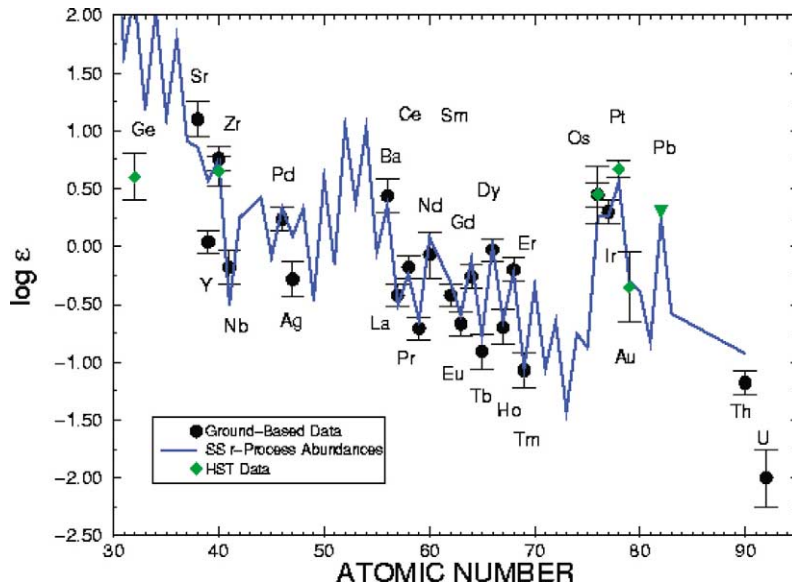


Fig. 2. Abundance comparison between the elements in BD 173248 [5] and a scaled solar system r-process (blue line) abundance distribution. Ground based data are indicated by black points, while data from the Hubble Space Telescope are indicated by green diamonds. In this star, the Fe/H ratio is less than 1/100 of that of the solar system.

entropy values, where the baryon density is the lowest. Finally, the remaining nuclei can capture neutrons and undergo a full neutron-capture r-process. Calculations have been performed [16] for a grid of entropies and proton to baryon ratios, trying to reproduce the abundance ratios of Ca–Ti–Cr observed in the EK-1-4-1 inclusion of the Allende meteorite. It is found that two different entropy conditions can reproduce simultaneously the observed abundance ratios: i.e.,  $^{48}\text{Ca}/^{46}\text{Ca} \simeq 250$ ,  $^{48}\text{Ca}/^{50}\text{Ti} \simeq 3$  and  $^{48}\text{Ca}/^{54}\text{Cr} \simeq 1$ .

At low entropy ( $S = 10k_B/\text{baryon}$ ), the Ca–Ti–Cr isotopes are synthesized in an  $\alpha$ -rich freeze out where essentially no free neutrons are available for subsequent neutron captures (pink arrows of Fig. 3 Top). The neutron-rich stable  $^{48}\text{Ca}$  and  $^{64}\text{Ni}$  are formed directly, as calculated in an earlier study of Type Ia supernova by Meyer et al. [17]. These supernovae are thermonuclear explosions of accreting white dwarfs in binary systems with high rates of H-accretion. The increasing mass of the white dwarf, consisting mainly of C and O, towards the Chandrasekhar mass-limit leads finally to contraction and a complete explosive disruption of the white dwarf. The major requirement to form these neutron-rich stable nuclei reside in the very low  $Y_e$  value. This value depends on the rate of electron captures in the pre-supernova core ( $e^- + p \rightarrow n + \nu_e$ ), the central density of the white dwarf and the propagation speed of the flame front [18].

At higher entropy ( $S = 150k_B/\text{baryon}$ ), a weak r-process is triggered by the presence of free neutrons after the charged-particle reactions freeze out. This process may occur in the high entropy bubble at the outer core of a type II supernova (SNII) [19]. Under such conditions,  $^{48}\text{Ca}$  is mainly generated by  $\beta$ -decay of the neutron-rich progenitor  $^{48}\text{Ar}$  (blue line in Fig. 3 top). Similarly, the progenitor of  $^{64}\text{Ni}$  would be possibly found at mass number  $A = 64$  in the Cr isotopic chain if the beta-decay time of  $^{64}\text{Cr}$  is shorter than its the neutron-capture time. In such a case, the  $^{64}\text{Cr}$  would act as a ‘turning point’, the neutron-capture flow being depleted to the higher  $Z$  chain. The location of these turning points for a stellar neutron-density of about  $5 \times 10^{20} \text{ cm}^{-3}$  is indicated by the red squares far off stability.

The two processes mentioned above produce considerably different patterns of abundances as a function of the mass number  $A$  (bottom part of Fig. 2). The global rate of  $^{48}\text{Ca}$  and  $^{64}\text{Ni}$  production is by far higher in the low entropy scenario. It is, therefore, very likely that the bulk  $^{48}\text{Ca}$  matter in our solar system has been produced by SNIa, which occur approximately 10 times more often than SNII. However, the observed isotopic anomalies of the EK-1-4-1 meteorite are not all reproduced by the low entropy scenario. In particular, the  $S = 10$  condition provides a somewhat low abundance of  $^{64}\text{Ni}$  as compared to  $^{48}\text{Ca}$ , a large overabundance of  $^{66}\text{Zn}$ , and no nuclei synthesized beyond  $A = 90$ . These three points are contradictory to the observations of the inclusions of the Allende meteorite [9,20,21]. Therefore, the high entropy scenario better fulfills the observations.<sup>1</sup> This calculation includes recent nuclear physics data for the neutron-rich progenitors. Since then, new results have been obtained far

<sup>1</sup> Only few pieces of the EK-1-4-1 inclusion are left for further analysis. It is planned to further study correlated anomalies including heavier species with new ionic nanoprobe.

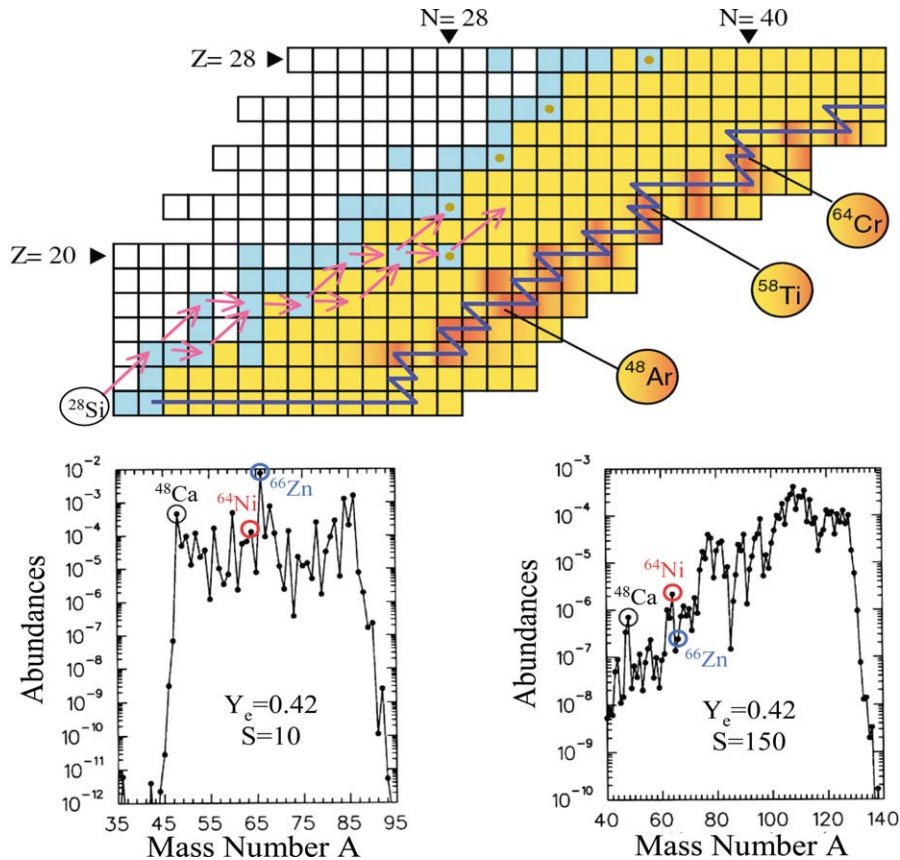


Fig. 3. Top: Part of the chart of the nuclides showing the location of stable nuclei (blue squares), of 'overabundant' isotopes in the EK-1-4-1 inclusion of meteorite (brown dot), and of the schematic nucleosynthesis paths for low (pink arrows) or high entropy (blue line) conditions. Bottom: Isotopic abundances calculated [16] for a proton-to-neutron ratio  $Y_e = 0.42$  with two different entropy conditions of  $S = 10$  (left), and  $S = 150 k_B/\text{baryon}$  (right).

from stability in the region where the progenitors of  $^{48}\text{Ca}$ ,  $^{58}\text{Fe}$ ,  $^{64}\text{Ni}$  and  $^{66}\text{Zn}$  should be found. These studies are depicted in the following sections.

### 3. The $N = 28$ region

#### 3.1. Beta-decay studies at GANIL

In order to better understand how  $^{46}\text{Ca}$  could be underproduced as compared to  $^{48}\text{Ca}$ , experiments have been performed at the GANIL accelerator in order to measure the  $\beta$ -decay half-lives of their neutron-rich progenitors. As production mechanism, the projectile fragmentation of a 60 A-MeV  $^{48}\text{Ca}$  (about one third the speed of light) beam was used onto a 140  $\mu\text{m}$ -thick  $^{58}\text{Ni}$  target. The LISE achromatic spectrometer operated to select the weakly produced fragments of interest among the total rate of nuclei produced in the collision (see a detailed example in the next section). About a decade ago, the  $\beta$ -decay properties  $T_{1/2}$  and delayed neutron emission probability  $P_n$  of the very neutron-rich  $^{43}\text{P}$ ,  $^{42,44,45}\text{S}$ ,  $^{44-45}\text{Cl}$  and  $^{47}\text{Ar}$  have been measured for the first time [22,23]. Some of these nuclei could emit a neutron in the  $\beta$ -decay process, with a probability  $P_n$ . In the case of  $^{43}\text{P}$ , this value is 100%, whereas in  $^{46}\text{Cl}$  it is 60%. Hence, the  $\beta$ -decay of  $^{46}\text{Cl}$  occurs preferentially to  $^{45}\text{Ar}$ .

Very surprising results were obtained from these studies. Compared to the model predictions which assumed a spherical shape for these  $N \simeq 28$  near magic nuclei, the experimental  $T_{1/2}$  were systematically shorter, by about a factor 3 for  $^{43}\text{P}$ , a factor 4 for  $^{45}\text{Cl}$ , and up to a factor 10 for  $^{44}\text{S}$ . These results were soon interpreted as a strong indication of the erosion of the  $N = 28$  closed-shell below  $^{48}\text{Ca}$ , leading to the onset of a strong quadrupole deformation for these nuclei [22,24]. These results have important consequences in nuclear physics and astrophysics. Although initially not predicted by any model and not

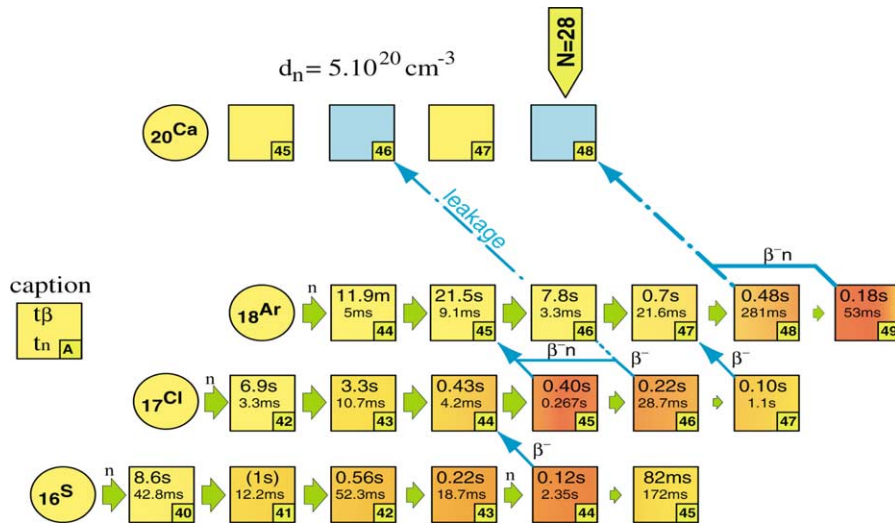


Fig. 4. Detailed view of the  $^{46}\text{Ca}$  and  $^{48}\text{Ca}$  region. The neutron-capture path is illustrated by the green arrows, whereas the location of the branching points is shown by the blue arrows. Measured  $\beta$ -decay half-lives (denoted here  $t_\beta$ ) are included in the first line of each square, the second line corresponds to calculated neutron-capture times assuming a mean neutron density of  $5 \times 10^{20} \text{ cm}^{-3}$  and a temperature of  $8 \times 10^8 \text{ K}$ .

accepted by the nuclear-structure community, these ideas were confirmed a few years after by both theories [25–29] and other experimental studies [30–33]. Even if not completely proven yet, this effect could be a direct consequence of the reduction of the spin-orbit interaction in neutron-rich nuclei. This would originate from the increase of surface diffuseness for these loosely bound neutron-rich nuclei. Related to the  $^{46,48}\text{Ca}$  anomalies, the shorter than predicted half-lives of  $^{44}\text{S}$  and  $^{45}\text{Cl}$  hinder further neutron-captures in the S and Cl chains, respectively [22]. The neutron-capture flow is partly depleted to the high- $Z$  chain prior to reach the mass number  $A = 46$  as shown in Fig. 4. For instance, at a neutron-density  $d_n = 5 \times 10^{20} \text{ cm}^{-3}$ ,  $t_n \gg t_\beta$  for  $^{44}\text{S}$ . As a result, very few  $A = 46$  neutron-rich progenitors of  $^{46}\text{Ca}$  are present in the S chain, and few from the Cl one. The remaining possibility is accounted for by the leakage-rate from the  $\beta$ -decay of  $^{46}\text{Ar}$ .

With the increase of the primary beam rate at GANIL by a factor of about 10, new  $\beta$ -decay measurements have been performed. The previous half-lives have been confirmed and those of  $^{46}\text{S}$ ,  $^{47}\text{Cl}$ ,  $^{48}\text{Ar}$  have been determined [34]. In the meantime, the very neutron-rich isotopes  $^{49,50}\text{Ar}$  have been studied at CERN/ISOLDE [35]. Thus, all  $\beta$ -decay lifetimes have been determined in the whole region where the progenitors of  $^{46}\text{Ca}$  and  $^{48}\text{Ca}$  are found.

Mass measurements have also been carried out at the  $N = 28$  shell closure below  $^{48}\text{Ca}$  with an accuracy better than 500 keV down to  $^{42}\text{Si}$  [36]. The mass-values rules the photodisintegration rate of nuclei ( $\gamma, n$ ) by the high blackbody-like photon flux prevailing at explosive stellar temperatures larger than  $10^9 \text{ K}$ .

### 3.2. Neutron-capture cross sections

Neutron-capture cross sections ( $\sigma_n$ ) have been measured for almost all stable nuclei, by irradiating target nuclei with neutron fluxes whose energy profile simulate the neutron spectrum in stars [37,10]. It was found from these studies that a drastic decrease of the neutron-capture cross section (by 2–3 orders of magnitude) occurs at the major closed shells, due to the complete filling of the neutron orbitals.

However, a direct determination of the neutron-capture cross section cannot be undertaken for short-lived radioactive species for which targets cannot be made. Alternative techniques are being envisaged by simulating the neutron capture process through a (d, p) transfer reaction. In such a case, a radioactive beam (of  $^{46}\text{Ar}$  for instance) impinges onto a deuteron target ( $\text{CD}_2$ ) in which it picks up a neutron. The signature of the reaction resides in the detection of protons which escape the target with energies which depend on the state to which the neutron has been captured. From this experiment, the energy of the states (bound or above the neutron energy threshold  $S_n$ ) and the spectroscopic factor  $S$  could be deduced. The spectroscopic factor describes the overlap between the intrinsic wave function of a given state – which is a linear combination of several orbitals – and a pure configuration. The  $\sigma_n$  value can subsequently be calculated from the (d, p) reaction using the formalism described by Kraussmann et al. [38] in the case of  $^{48}\text{Ca}$  for which both the (n,  $\gamma$ ) and (d, p) reactions have been used.

The  $\sigma_n$  value  $^{46}\text{Ar}(n, \gamma)^{47}\text{Ar}$  is a key parameter, since it fixes the leakage of the neutron-capture flow at  $A = 46$  in the Ar chain. The  $^{46}\text{Ar}$  nucleus is at the  $N = 28$  shell closure, where a sudden drop of the neutron-separation energy – which is the

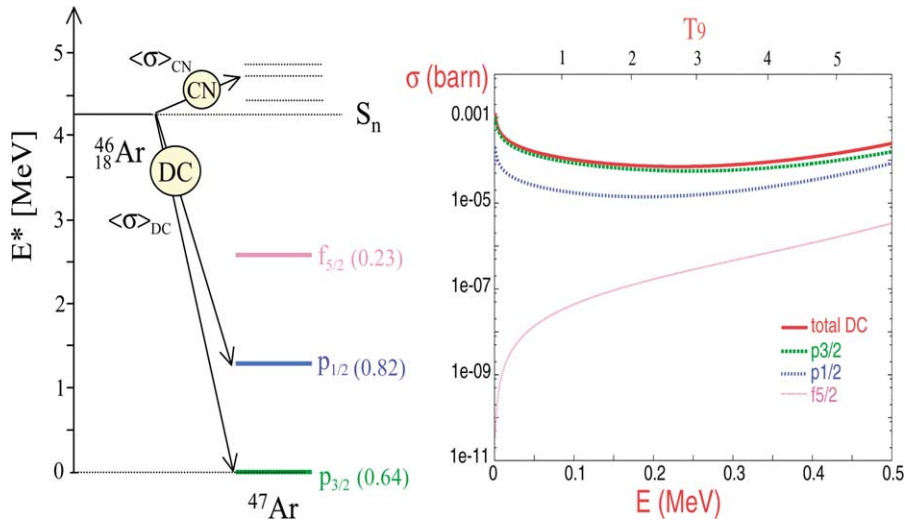


Fig. 5. Left: Shell model calculation of the level scheme of  $^{47}\text{Ar}$  as a function of the energy  $E^*$ . The main levels which contribute to the neutron-capture are represented with their respective angular momenta  $\ell_J$  and spectroscopic factors (in parenthesis). Right: Calculated  $\sigma_n$  value for the three levels shown in the left part; the total contribution is shown in red.

Q-value in the case of a neutron-capture cross section – is expected, even if the shell closure is partially eroded. Consequently, the  $\sigma_n$  value of  $^{46}\text{Ar}(n, \gamma)^{47}\text{Ar}$  should be small as compared to neighboring nuclei. As schematically shown in Fig. 5 left, the neutron-capture could occur through a compound nucleus (CN) or directly to bound states (DC). In the CN case, the neutron-capture occurs at energies close to the  $S_n$  value through the formation of a compound nucleus, which subsequently de-excites by photon emissions. To get a feeling of how to calculate the  $\sigma_n$  value in  $^{46}\text{Ar}$ , we could be inspired by what has been achieved in the case of the stable isotone  $^{48}\text{Ca}$ . The experimental neutron-capture cross section on  $^{48}\text{Ca}$  has been determined to be of 0.55(9) mb [11]. It was pointed out that 95% of the cross section is of DC origin [38]. The reason for a very small CN contribution can be traced back to the low nuclear level density at  $N = 28$ , providing few possibilities for the formation of a compound nucleus. The high DC value originates from the intrinsic nuclear structure of  $^{49}\text{Ca}$ , which exhibits a low angular momentum ground state. For neutron energies below 100 keV – corresponding to a stellar temperature of about  $1.2 \times 10^9$  K, the  $\sigma_n$  is strongly inhibited by the centrifugal barrier of the orbital to which the neutron could be captured. For instance, the  $\sigma_n$  value to a  $\ell = 3\hbar$  state (denoted f) is 1000 times lower than to a lower angular momentum state of  $\ell = 1\hbar$  (denoted p). Shell model calculations have been performed by F. Nowacki to determine the level scheme of  $^{47}\text{Ar}$ , the energy of the excited states, their angular momenta and spectroscopic factors  $S$  (Fig. 5 left). The theoretical  $\sigma_n$  value is given by the sum over each final state to which the neutron capture could occur:

$$\sigma_n \simeq \sum_i S_i \sigma_i^{DC}. \tag{1}$$

The levels which contribute to the largest extent are represented and labelled by their  $\ell_J$  configuration, J being the total angular momentum which include the intrinsic spin value of the solitary neutron. It is seen that the neutron capture to the ground state  $p_{3/2}$  ( $\ell = 1$ ) is by far the largest (Fig. 5 right). The presence of this low- $\ell$  orbital available in  $^{47}\text{Ar}$  is speeding up the neutron-capture rate as compared to what occurs normally at shell closures. This feature has the important consequence to reduce drastically the leakage at  $A = 46$ , the neutron-capture time being shorter than the beta-decay time by a factor of about 2000 at a stellar neutron-density of  $5 \times 10^{20} \text{ cm}^{-3}$ .

We have used the measured  $\beta$ -decay rates and calculated neutron capture cross sections to simulate a neutron-capture  $\beta$ -decay process and determine the  $^{48}\text{Ca}/^{46}\text{Ca}$  ratio. The variation of this ratio as a function of the stellar neutron-density and of the time scale of the process is exemplified in Fig. 6. The seed abundance was taken as solar. This parametric study does not self-consistently follow a stellar explosion but specifies the range of neutron densities which could account for such a high ratio.<sup>2</sup> A large  $^{48}\text{Ca}/^{46}\text{Ca}$  ratio, though not as large as that observed in EK-1-4-1, could be found for neutron fluxes in the range of  $8 \times 10^{-5} \text{ mol}\cdot\text{cm}^{-3}\cdot\text{s}$ . Short irradiation timescales of  $\tau \leq 100 \text{ ms}$  – corresponding to neutron densities  $d_n \simeq 5 \times 10^{20} \text{ cm}^{-3}$

<sup>2</sup> In particular, the abundance pattern of the seed nuclei may differ from that of the  $S = 10$  entropy condition in which they were formed by  $\alpha$  captures.

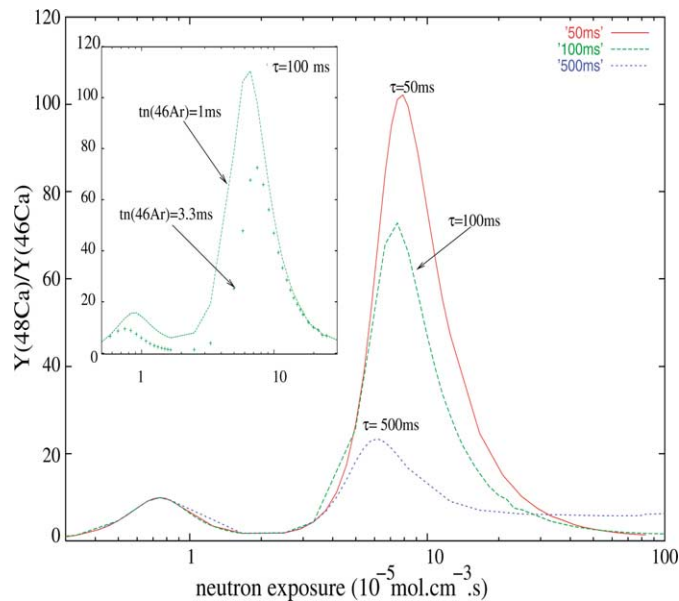


Fig. 6. Abundance ratio  $^{48}\text{Ca}/^{46}\text{Ca}$  as a function of neutron flux for various combinations of neutron densities and exposure times  $\tau$  in milliseconds. Shown in the insert is the variation of  $^{48}\text{Ca}/^{46}\text{Ca}$  ratio when increasing the  $\sigma_n$  of  $^{46}\text{Ar}$  by a factor 3.

– better account for a high ratio. By increasing the irradiation time, the neutron-capture flow from the S and Cl chains have time to be depleted in the Ar chain, thus eventually enriching  $^{46}\text{Ca}$  (see also Fig. 4). A smaller neutron-capture cross section at the  $^{45}\text{Cl}$  would considerably hinder the feeding from the Cl chain. The sensitivity of the  $^{48}\text{Ca}/^{46}\text{Ca}$  ratio to the  $\sigma_n$ -value of  $^{46}\text{Ar}$  is shown in the inset of Fig. 6; short  $\sigma_n$ -value allows for longer irradiation timescales.

It is interesting to see whether a similar neutron-capture  $\beta$ -decay process could also account for the production of the heavier- $Z$  stable nuclei  $^{58}\text{Fe}$  and  $^{64}\text{Ni}$ . The study of their neutron-rich progenitors, which should lie in the Sc–Cr isotopic chains, is essential to achieve this goal.

#### 4. The $N = 40$ region

##### 4.1. Beta-decay studies

The study of neutron-rich  $^{21}\text{Sc}$ – $^{27}\text{Co}$  nuclei has been started at GANIL in 1997. Three dedicated experiments have been performed, using the fragmentation of different primary beams of  $^{65}\text{Cu}$  [39,40],  $^{86}\text{Kr}$  [41] and  $^{76}\text{Ge}$  [42]. Beta-decay studies of more than 40 nuclei, which span from about 8 to 15 mass units away from the valley of stability, have been achieved during these experiments. The aim of these study was twofold: first,  $\beta$ -decay half-life  $T_{1/2}$  is one of the easiest nuclear property accessible for weakly produced nuclei, and the very first nuclear structure information could be extracted from its value and from the  $\gamma$ -lines following the  $\beta$ -decay. Second, we wished to reach nuclei which could play an important role in a weak r-process nucleosynthesis, with neutron-densities of up to  $10^{21}\text{ cm}^{-3}$ . Until 1997, only predictions were available in order to fill the gap between nuclei close to stability and nuclei 15 mass units away.

A similar experimental technique has been applied for the three experiments mentioned above. In the last one, neutron-rich  $^{57,58}_{21}\text{Sc}$ ,  $^{58-60}_{22}\text{Ti}$ ,  $^{60-63}_{23}\text{V}$ ,  $^{62-66}_{24}\text{Cr}$ ,  $^{64,68}_{25}\text{Mn}$  and  $^{68-70}_{26}\text{Fe}$  isotopes have been produced at GANIL by the fragmentation of a 61.8 A.MeV  $^{76}\text{Ge}^{30+}$  beam, of mean intensity 1  $\mu\text{A}$ , onto a  $^{58}\text{Ni}$  target of 118  $\mu\text{m}$  thickness. The nuclei of interest were separated by the LISE3 achromatic spectrometer whose magnetic rigidity was tuned to optimize the transmission rate of these very neutron-rich nuclei (Fig. 7 left). The nuclei transmitted through the spectrometer were identified by means of 3 consecutive 300, 300, 1500  $\mu\text{m}$  silicon detectors. The two first served for the energy loss and time-of-flight measurements. The last, into which the nuclei were implanted, determined their residual energies. It was divided in sixteen 3 mm wide, 46 mm height vertical strips. The rate of nuclei implanted was about one per second in total. An identification plot of the nuclei transmitted is shown in Fig. 7 right.

Each time a nucleus was implanted in one of the strips, the primary beam was switched off during 1 second to collect the beta-rays ( $e^-$ ) of its decay ( $n \rightarrow p + e^- + \nu_e$ ) in the same strip. Hence, a very good space correlation between the  $\beta$ -rays and the

precursors implants is obtained, reducing the  $\beta$ -background rate originating from radioactivities of long lived grand-daughter nuclei. Beta-decay time spectra correlated with the implantation of Ti and Cr isotopes are shown in Fig. 8. Results obtained in the Sc, V, Mn, Fe and Co chains could be found in [42,45]. The study of the Mn isotopes has also been achieved at CERN/ISOLDE using a somewhat different experimental technique [44]. The half-lives of  $^{64-68}\text{Mn}$  are in very good accordance between both experiments, bringing strong confidence in the present measurements.

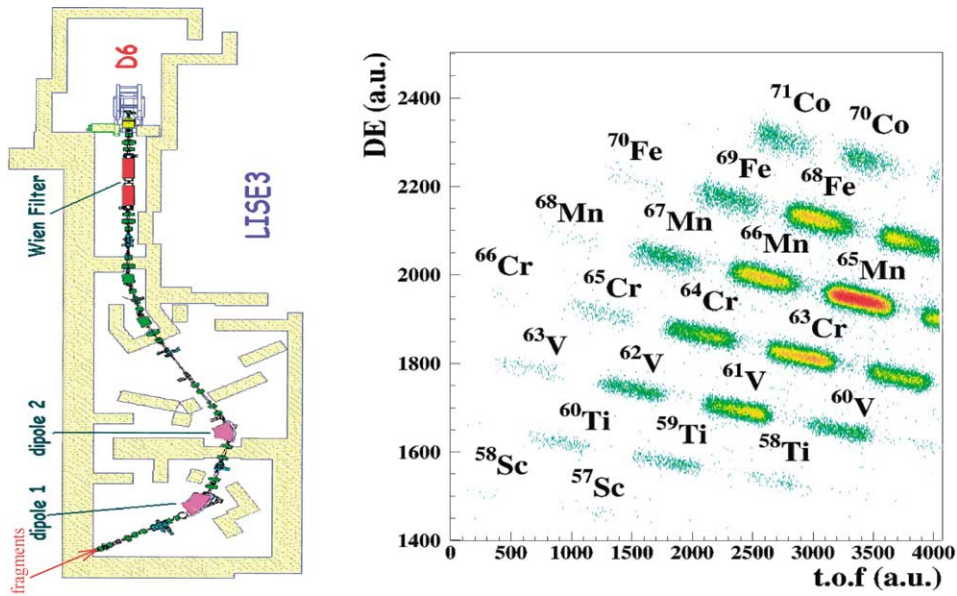


Fig. 7. Left: Schematic view of the LISE3 spectrometer (44 meters length) in which the nuclei of interest are selected after their production in the target. Right: Energy loss (DE) versus time of flight (t.o.f) identification plot of the nuclei transmitted through the spectrometer.

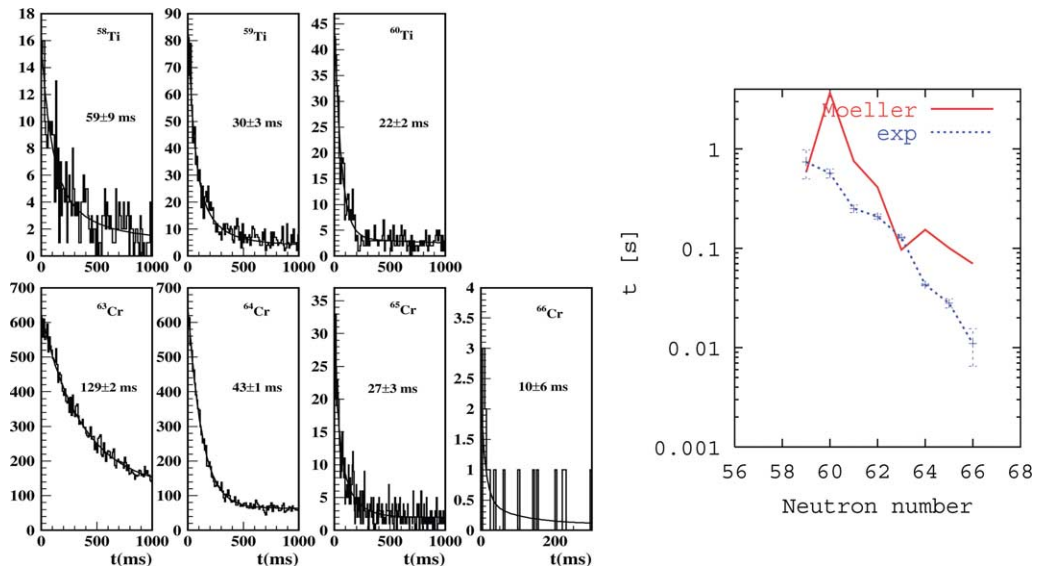


Fig. 8. Left: Beta-decay time-spectra of neutron-rich Ti and Cr isotopes. The corresponding half-lives are included for each isotope. Right: Comparison between calculated half-lives [43] (full line) and experimental ones (dashed line) in the Cr isotopic chain.

A comparison between the experimental and calculated [43]  $\beta$ -decay half-lives of Cr isotopes is shown in Fig. 8 right. The theoretical half-life  $T_{1/2}$  is given by the integral of the beta strength function  $S_\beta$  over the levels available in the daughter nucleus at an energy  $E^*$ :

$$1/T_{1/2} \simeq \int_0^{Q_\beta} S_\beta(Q_\beta - E^*)^5 dE^*. \quad (2)$$

$S_\beta$  is given by the selection rules of the  $\beta$ -decay operator between initial (mother) and final states (daughter nucleus),  $Q_\beta$  is the maximum energy available in the transition. The theoretical values of Möller differ beyond  $N = 39$  by up to an order of magnitude due to the persistence of deformation at  $N = 40$ , not predicted by the model. Möller finds that the potential-energy surfaces are very soft in the  $^{64}\text{Cr}$  nucleus, with two shallow minima of different shapes separated by barriers of only 100 keV height. It is, therefore, hardly possible to determine which of these minima is the ground state. The choice of one of these could change the  $S_\beta$  and hereafter the  $T_{1/2}$ -value by a factor of about 4. In addition to this, the  $Q_\beta$  value predictions differ by up to 3 MeV between different models. These uncertainties are making half-life predictions very difficult in this region.

In order to get a more profound understanding of the nuclear structure of these unstable nuclei, we have looked for their  $\gamma$ -rays. For this purpose, four Ge detectors were placed around the implantation detector for the search of the main  $\gamma$ -transitions following the  $\beta$ -decay. Beta-gated  $\gamma$ -ray spectra of  $^{60}_{23}\text{V}$  and  $^{62}_{23}\text{V}$  exhibit  $\gamma$ -lines at 646(1) keV and 446(1) keV, corresponding to the  $2^+ \rightarrow 0^+$  transitions in  $^{60}_{24}\text{Cr}$  and  $^{62}_{24}\text{Cr}$ , respectively [42]. The first excited state of even-even nuclei is generally of quadrupole origin, corresponding to (particle-hole) excitations between filled and vacant orbitals. This excited mode could be attributed to vibration or rotation if the nucleus ground-state is spherical or deformed, respectively. A high  $2^+$  energy (2 MeV and higher) characterizes closed-shell nuclei for which a high energy is required to promote the nucleus into an excited state. Very small values are often signatures of deformed nuclei. By comparing the  $2^+$  energies in the Cr and Ni isotopic chains, it is possible to deduce how the structure of these nuclei evolves when approaching the  $N = 40$  sub-shell closure (Fig. 9). This is discussed in the next subsection.

These Ge detectors were also used to detect delayed  $\gamma$ -transitions following the decay of an isomeric excited state. Indeed, it is possible that nuclei could be trapped into an isomeric state subsequently to their formation in the collision between the primary beam and the target. This isomer could survive through the 1  $\mu\text{s}$  flight-time in the spectrometer and eventually  $\gamma$ -decay at the implantation detector. In the case of  $^{59}\text{Ti}$ , two isomers were found [46], attributed to E2 (electric quadrupole) and M2 (magnetic quadrupole) origins. An explanation of this striking feature will be suggested in the following.

#### 4.2. Nuclear structure at the $N = 40$ subshell closure

Several experiments have been performed at this  $N = 40$  sub-shell closure, aiming to obtain the energy of the orbitals around the  $^{68}\text{Ni}$  nucleus and the size of the  $N = 40$  gap [47–55]. In addition to this, the Coulomb excitation of  $^{68}\text{Ni}$  has brought some important information about the amount of collectivity (particle-hole excitations) which could develop in this nucleus [56]. In such experiment, a secondary beam of  $^{68}\text{Ni}$  is passing through a Pb target where it could be excited to its first excited state by the Coulomb field of the target nuclei. In the case of  $^{68}\text{Ni}$ , this Coulomb excitation rate to the  $2^+$  state B(E2) is extremely small; the smallest in all hitherto studied Ni isotopes. This extremely small rate of excitation across  $N = 40$  could be explained by the change of parity between filled and valence states in  $^{68}\text{Ni}$ , as shown in Fig. 9 right. The filled states, denoted by  $p_{1/2}$  and  $f_{5/2}$ , have a negative parity with an orbital momentum  $\ell = 1$  and 3, respectively. The valence states g and d have a positive parity because of their even  $\ell$ -values of 4 and 2, respectively. By crossing the  $N = 40$  sub-shell, only parity breaking excitations could in principle occur – therefore excluding quadrupole ones – except if a pair of neutrons is promoted to the higher state. Superfluid effects somewhat counteracts this parity-induced hindrance factor. Nuclear superfluidity can be characterized by pair-scattering to valence states. This effect scales approximately with the occupation probability of each level, e.g., as  $2J + 1$ . Therefore, a pair of nucleon from fp orbits is in average scattered to the  $g_{9/2}$  valence state, bringing back few quadrupole excitations in the fp space which is not completely filled anymore. Most of the properties of  $^{68}\text{Ni}$  can be explained with shell model calculations within the f, p and g valence space, denoted further as fpg. In particular, the B(E2) and  $2^+$  energy trend, can be explained throughout the Ni isotopic chain within the fpg space.

For our purpose, it is important to predict the evolution of this neutron sub-shell closure below  $^{68}\text{Ni}$  to determine the neutron-capture rates around the  $^{64}\text{Cr}_{40}$  and  $^{58}\text{Ti}_{36}$  isotopes. As shown in the  $N = 28$  closed shell region, the nuclear structure could have a dramatic impact on the neutron-capture rate. It is clearly seen from Fig. 9 left that a major nuclear structure change has occurred between the Ni and Cr isotopic chains. Instead of a sharp rise of the  $2^+$  at  $N = 40$  in the Ni chain (dashed violet line), a steady decrease is found in the Cr chain (blue line). This later feature in the Cr chain can neither be explained by using the fp (red line) nor the fpg (green line) valence space [42].

The  $^{64}\text{Cr}_{40}$  nucleus contains 4 protons less than  $^{68}\text{Ni}$ . These 4 protons have been removed from the  $f_{7/2}$  orbital, which is filled by 8 protons in  $^{68}\text{Ni}$ . At  $N = 40$ , the neutron orbital  $f_{5/2}$  is also completely filled. The strongly attractive proton-neutron

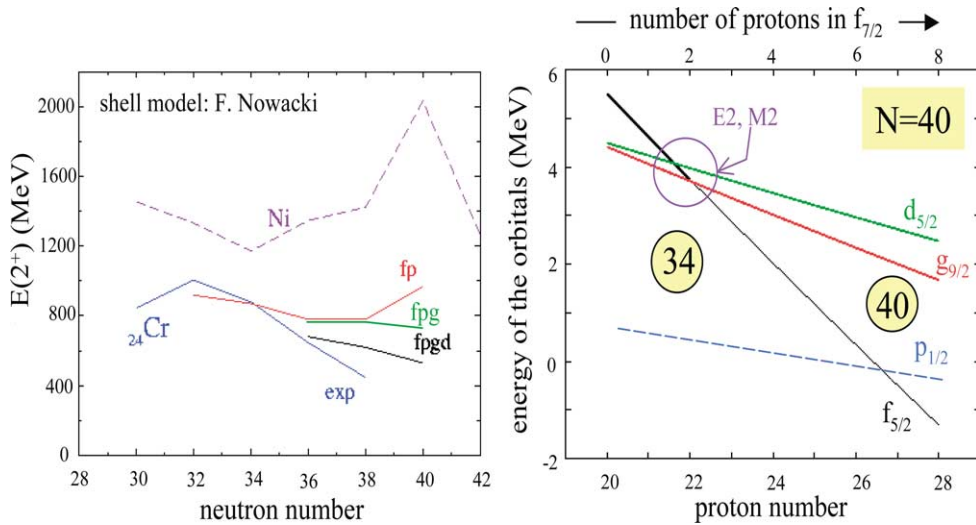


Fig. 9. Left: Experimental and calculated energies of the first  $2^+$  excited state in the Ni and Cr isotopic chains. The curves labelled with fp, fp+g, and fp+g+d for Cr isotopes correspond to shell model calculations assuming valence spaces which progressively include the g and d orbitals. Right: Evolution of the energy of the neutron orbitals for the  $N = 40$  isotones as a function of the proton number.

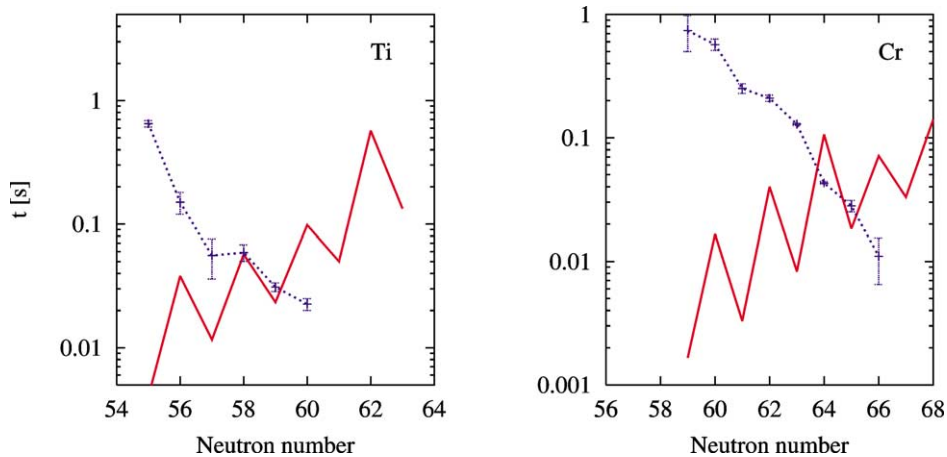


Fig. 10. Comparison between neutron-capture times (red line) and experimental  $\beta$ -decay times (dotted blue) in the Ti (left) and Cr (right) isotopic chains. These values have been determined using a neutron density of  $6 \times 10^{20} \text{ cm}^{-3}$ .

interaction between these two orbitals of same angular momentum and opposite spin value drastically lowers the  $f_{5/2}$  orbital energy, as shown in Fig. 9 right [42]. In  $^{68}\text{Ni}$ , the energy of the  $f_{5/2}$  orbital is minimum, whereas this orbital raises when decreasing the proton number, eventually crossing the g and d ones in Ti. Consequently, a sub-shell closure is present at  $N = 40$  for  $^{68}\text{Ni}$  with a clear separation between fp and g orbitals. In the neutron-rich Cr isotopes, this gap has shrunk and the g, d orbitals lie closer in energy. The presence of these valence orbitals of  $J, J - 2$  spins brings a large amount of quadrupole excitations [57,42]. The presence of E2 and M2 isomers in  $^{59}\text{Ti}$  can be traced back through the crossing of the  $f_{5/2}$ ,  $g_{9/2}$  and  $d_{5/2}$  orbitals.

The half-lives of the Ti and Cr isotopes reported in Fig. 8 are compared to neutron-capture times calculated by Rauscher et al. [58] for a neutron density condition of  $d_n = 6.10^{20} \text{ cm}^{-3}$  (see Fig. 10). So far, these  $\sigma_n$  calculations have been performed in the Ti and Cr nuclei using the deformation parameters and single particle levels calculated by Möller et al. [43].<sup>3</sup> From Fig. 10,

<sup>3</sup> The conclusions drawn below may be changed by taking into account the evolution of the energy of the orbitals with the proton-neutron interactions and the deformation at  $N = 40$ . It is expected that the presence of high- $\ell$  valence orbitals should lower the cross section.

it is seen that a turning point occurs in the Cr chain at  $^{64}\text{Cr}$ , the beta-decay time of  $^{64}\text{Cr}$  being shorter than its neutron capture time. As a consequence, the Cr chain will mainly feed the  $^{64}\text{Ni}$  isotope, and to a much weaker extent the  $^{66}\text{Zn}$  isotope since the major part of the neutron-capture flow is already depleted at the mass number 64. Since no branching point at  $A = 66$  is expected in any of the higher  $Z$  isotopic chains, it is surmised that the  $^{66}\text{Zn}$  will be underproduced by this process. (In the odd- $Z$  chains of Sc, V, and Mn, the main branching points are odd- $A$  nuclei, and in the Fe chain the branching occurs at a larger mass, i.e., around  $^{72}\text{Fe}$ ). Similarly, a branching point occurs at  $^{58}\text{Ti}$ , which would be reinforced at a somewhat weaker neutron density. The most probable progenitor of the neutron-rich stable  $^{58}\text{Fe}$  is  $^{58}\text{Ti}$ . This process naturally explains large correlated overabundances of  $^{58}\text{Fe}$  and  $^{64}\text{Ni}$ , and an underabundance of  $^{66}\text{Zn}$ . The ‘weak’ r-process is, therefore, a promising scenario to account for the observed isotopic anomalies in certain inclusions of meteorites.

## 5. Conclusions

Possible astrophysical scenarios which account for the observed abundances of the neutron-rich  $^{48}\text{Ca}$  to  $^{66}\text{Zn}$  have been discussed. It has been concluded they can be produced at high temperature and density conditions with two different entropy conditions. At  $S \simeq 10$ , these nuclei are formed directly from charged particles (mainly  $\alpha$ 's) reactions with few neutrons only. Such conditions are typically found in Type Ia supernovae, whereas  $S \simeq 150$  rather mimics the outer core of type II supernovae conditions. SNIa produces  $^{48}\text{Ca}$  by about 2 orders of magnitude larger than SNII. Moreover, SNIa events occur approximately ten times more than SNII. Consequently, SNIa have probably synthesized and ejected the bulk  $^{48}\text{Ca}$  material in the solar system, as outlined by Meyer et al. [17]. However, the  $S \simeq 150$  calculations reproduce simultaneously the overall agreement with the isotopic abundances in EK-1-4-1 ranging from  $^{48}\text{Ca}$  to the heavier isotopes Nd and Sm. This feature suggests that the EK-1-4-1 condensate may have been synthesized during a specific SNII event. In such a case, the stable  $^{48}\text{Ca}$ ,  $^{58}\text{Ti}$  and  $^{64}\text{Ni}$  are synthesized in a neutron-capture  $\beta$ -decay process by neutron-rich progenitors. Recent experimental nuclear physics data have been obtained in the  $N = 28$  and  $N = 40$  regions, extending in particular the  $\beta$ -decay rates 10–15 mass units far from stability. Remarkable features can be emphasized in both regions.

The progressive erosion of the  $N = 28$  closed shell is partly responsible for the deformation of the Cl and S nuclei below  $^{48}\text{Ca}$ , leading to unexpectedly ‘short’  $T_{1/2}$  at  $^{44}\text{S}$  and  $^{45}\text{Cl}$ . These nuclei, therefore, act as ‘turning points’ and reduce the abundance of  $A = 46$  isotopes in the S and Cl chains, respectively. In the Ar chain, the amount of  $^{46}\text{Ca}$  production is governed by the leakage of the neutron-flow at  $^{46}\text{Ar}$ . It has been shown that the intrinsic shell structure of  $^{47}\text{Ar}$  ( $p_{3/2}$   $\ell = 1$  ground state orbital) favors the  $^{46}\text{Ar}$  neutron-capture and subsequently speed up the neutron-capture flow at  $N = 28$ . The  $^{48}\text{Ca}$  is produced mainly by the  $^{48}\text{Ar}$  and  $^{49}\text{Ar}$  progenitors.

The proton-neutron interaction  $\pi f_{7/2} - \nu f_{5/2}$  brings a re-ordering of the neutron orbitals below  $^{68}\text{Ni}$ . Consequently, the valence orbitals exhibit high angular momenta ( $\ell \geq 3$ ) mainly, leading to strong neutron-capture hindrances in the region where the progenitors of  $^{58}\text{Fe}$  and  $^{64}\text{Ni}$  should be found. By using similar neutron-density conditions as in the  $^{48}\text{Ca}$  mass region, it is found that branching points occur in the Ti and Cr chains at  $^{58}\text{Ti}$  and  $^{64}\text{Cr}$ , respectively. This makes these nuclei very likely progenitors of the stable  $^{58}\text{Fe}$  and  $^{64}\text{Ni}$  in this neutron-capture  $\beta$ -decay scenario.

The perspectives concerning this study are multiple. From the observational point of view, it is conceivable that lighter r-nuclei could be observed in the UMP stars. In addition to this, recent observations have demonstrated the possibility to access to isotopic abundances of Ba and Eu. When extended to lighter elements, these data could bring a new insight on the origin and existence of ‘weak’ r-process. At present, the EK-1-4-1 inclusion has been analyzed by the standard technique: the elements are first chemically separated from the sample, and their isotopic content is provided by mass spectrometry. A re analysis of the piece of EK-1-4-1 inclusion by the ionic nanoprobe is envisaged soon, with the aim of extending the Ca–Ti–Cr observations to heavier elements observed in the UMP stars. This would bring a much clearer idea of the nucleosynthesis process (low or high entropy scenario) which has produced these isotopic anomalies. From the nuclear physics point of view, neutron-capture cross section of the neutron-rich  $^{44,46}\text{Ar}$  will be determined soon. This will bring a better constraint on the stellar conditions which could account for large  $^{48}\text{Ca}/^{46}\text{Ca}$  ratio.

## Acknowledgements

O.S. wishes to thank all colleagues who participate to the experiments reported here. Valuable discussions with M. Girod, H. Grawe and F. Nowacki are also greatly acknowledged. This work was partially supported by the Swiss NSF (grant 2000-061031.02). T.R. acknowledges support by a PROFIL professorship from the Swiss NSF (grant 2024-067428.01).

## References

- [1] E. Burbidge, G. Burbidge, W. Fowler, F. Hoyle, *Rev. Mod. Phys.* 29 (1957) 546.
- [2] C. Sneden, et al., *Ap. J.* 496 (1998) 235.
- [3] C. Sneden, et al., *Ap. J.* 533 (2000) L139.
- [4] J.W. Truran, et al., *Nucl. Phys. A* 688 (2001) 330c.
- [5] J. Cowan, et al., *Ap. J.* 572 (2002) 861.
- [6] T. Lee, et al., *Ap. J.* 220 (1978) L21.
- [7] F.R. Niederer, et al., *Ap. J.* 240 (1980) L73.
- [8] J. Völkening, D.A. Papanastassiou, *Ap. J.* 347 (1989) L43.
- [9] J.L. Birck, G.W. Lugmair, *Earth Planetary Sci. Lett.* 90 (1988) 131.
- [10] F. Käppeler, *Prog. Nucl. Part. Phys.* 43 (1999) 419.
- [11] F. Käppeler, G. Walter, G.J. Mathews, *Ap. J.* 291 (1985) 319.
- [12] K.L. Kratz, et al., *Ap. J.* 403 (1993) 216.
- [13] B. Pfeiffer, et al., *Nucl. Phys. A* 693 (2001) 282.
- [14] J. Wasserburg, M. Busso, R. Gallino, *Ap. J.* 466 (1996) L109.
- [15] C. Freiburghaus, et al., *Ap. J.* 516 (1999) 381.
- [16] K.L. Kratz, et al., *Mem. Soc. Astronom. Ital.* 72 N2 (2001) 453.
- [17] B.S. Meyer, et al., *Astroph. J.* 462 (1996) 825.
- [18] F. Brachwitz, *Ap. J.* 536 (2000) 934.
- [19] B.S. Meyer, et al., *Astroph. J.* 399 (1992) 656.
- [20] R.D. Loss, G.W. Lugmair, *Astroph. J.* 360 (1990) L59.
- [21] G.W. Lugmair, et al., *Lunar and Planetary Sci. IX* (1978) 672.
- [22] O. Sorlin, et al., *Phys. Rev. C* 47 (1993) 2941.
- [23] O. Sorlin, et al., *Nucl. Phys. A* 583 (1995) 763.
- [24] K.-L. Kratz, et al., *Phys. Blätter* 51 (1995) 183.
- [25] T.R. Werner, et al., *Phys. Lett. B* 335 (1994) 259.
- [26] J. Retamosa, et al., *Phys. Rev. C* 55 (1997) 1266.
- [27] G.A. Lalazissis, et al., *Phys. Rev. C* 60 (1999) 014310.
- [28] P.-G. Reinhard, et al., *Phys. Rev. C* 60 (1999) 014316.
- [29] S. Péru, M. Girod, J.F. Berger, *Eur. Phys. J. A* 9 (2000) 35.
- [30] H. Scheit, et al., *Phys. Rev. Lett.* 77 (1996) 3967.
- [31] T. Glasmacher, et al., *Phys. Lett. B* 395 (1997) 163.
- [32] F. Sarazin, et al., *Phys. Rev. Lett.* 84 (2000) 5062.
- [33] D. Soehler, et al., *Phys. Rev. C* 66 (2002) 054302.
- [34] S. Grévy, *Proceedings of the International Symposium on Physics of Unstable Nuclei, Halong Bay, Vietnam, November 20–25, 2002.*
- [35] L. Weissmann, private communication.
- [36] H. Savajols, private communication.
- [37] Z.Y. Bao, et al., *At. Data Nucl. Data Tables* 76 (2000) 70.
- [38] E. Kraussmann, et al., *Phys. Rev. C* 53 (1996) 469.
- [39] O. Sorlin, et al., *Nucl. Phys. A* 632 (1998) 205.
- [40] T. Dörfler, et al., *Phys. Rev. C* 54 (1996) 2894.
- [41] O. Sorlin, et al., *Nucl. Phys. A* 669 (2000) 351.
- [42] O. Sorlin, et al., *Eur. Phys. J. A* 16 (2003) 55.
- [43] P. Möller, J.R. Nix, K.-L. Kratz, *At. Data Nucl. Data Tables* 66 (1997) 131.
- [44] M. Hannawald, et al., *Phys. Rev. Lett.* 82 (1999) 1391.
- [45] O. Sorlin, et al., *Proceedings of the 17th Divisional Conference on Nuclear Physics in Astrophysics, Debrecen, Nucl. Phys. A* (2003) in print.
- [46] I. Matea, Ph.D. thesis work, Univ. de Caen, private communication.
- [47] M. Bernas, et al., *Phys. Rev. Lett.* 67 (1991) 3661.
- [48] T. Pawlat, et al., *Nucl. Phys. A* 574 (1994) 623.
- [49] R. Broda, et al., *Phys. Rev. Lett.* 74 (1995) 868.
- [50] H. Grawe, et al., *Prog. Part. Nucl. Phys.* 38 (1997) 15.
- [51] R. Grzywacz, et al., *Phys. Rev. Lett.* 81 (1998).
- [52] L. Weissman, et al., *Phys. Rev. C* 59 (1999) 2004.
- [53] W.F. Mueller, et al., *Phys. Rev. Lett.* 83 (1999) 3613.
- [54] W.F. Mueller, et al., *Phys. Rev. C* 61 (2000) 054308.
- [55] O. Sorlin, *Nucl. Phys. A* 682 (2001) 183c.
- [56] O. Sorlin, et al., *Phys. Rev. Lett.* 88 (2002) 092501.
- [57] A.P. Zuker, et al., *Phys. Rev. C* 52 (1995) R1741.
- [58] T. Rauscher, et al., in: M. de Saint Simon, O. Sorlin (Eds.), *Proceedings of the ENAM95 Conference, Frontières, Arles, France, June 1995*, p. 683.